ISSN 1063-7710, Acoustical Physics, 2016, Vol. 62, No. 3, pp. 319–327. © Pleiades Publishing, Ltd., 2016.
Original Russian Text © A.I. Belov, G.N. Kuznetsov, 2016, published in Akusticheskii Zhurnal, 2016, Vol. 62, No. 3, pp. 308–317.

OCEAN ACOUSTICS.
HYDROACOUSTICS

Direction Finding and Suppression of Vector-Scalar Sound Signals in Shallow Water Taking into Account Their Correlation and Mode Structure

A. I. Belov and G. N. Kuznetsov

Wave Research Center, Prokhorov General Physics Institute, Russian Academy of Sciences, ul. Vavilova 38, Moscow, 119991 Russia

e-mail: skbmortex@mail.ru

Received April 4, 2015

Abstract—The correlation of low-frequency sound signals from towed tonal low-frequency sources at the output of the scalar and vector channels is studied in shallow water. The correlation of the scalar field and signal received by a horizontally oriented vector receiver on average is 0.92–0.99; correlation with the signal received by a vertical vector receiver decreases to 0.66–85. When scalar fields or horizontal projections of the vibration velocity vector with application of the aperture synthesis algorithm are used, 3–5 normal waves are isolated; when the vertical component is used, 7–9 modes. It is demonstrated that the high signal correlation ensures direction-finding accuracy and suppression of strongly noise-emitting moving sources by 20–30 dB or more if the cardioid is directed at the source according to the zone of the minimum.

Keywords: correlation of scalar and vector sound fields, wave spectra, direction finding and suppression of a noise-emitting source

DOI: 10.1134/S1063771016030039

INTRODUCTION

The efficiency of detecting weak signals on a noise background using scalar arrays depends on the array characteristics, the signal/noise ratio at a single hydrophone, and the spatial correlation of signals and noise at the aperture of the array. The amplification coefficient (AC) of the array, by definition, is calculated as the signal/noise ratio (S/N) at the array output to the signal/noise ratio (s/n) at the output of one element. When equating $S_i = S_j$, $N_i = N_j$, $s_i = s_j$, $n_i = n_j$ (i, j are the numbers of receivers in the array), we can write the expression for the AC of the array in simplified form [1]:

$$\mathrm{AC} = 10\log\frac{\overline{S^2}/\overline{N^2}}{\overline{s^2}/\overline{n^2}} = 10\log\left[\sum_i\sum_j(\rho_s)_{ij}\Big/\sum_i\sum_j(\rho_n)_{ij}\right].$$

As a result, amplification of the array depends on the sum of the mutual correlation coefficients for a signal $(\rho_s)_{ij}$ and noise $(\rho_n)_{ij}$ for all pairs of elements, which can be formed from the overall number of array elements.

To detect signals using vector scalar arrays, it is necessary to have additional information on the of signal and noise correlation between the vector components V_x, V_y, and V_z and the scalar component P.

If P and V_x, V_y, V_z are measured synchronously and at one point, then for wideband vector scalar signals it is possible to use the frequency dependences of the normalized coherency function [2]:

$$K_l(\omega) = \frac{|S_{PV_l}(\omega)|}{\sqrt{S_{P^2}(\omega)S_{V_l^2}(\omega)}};\quad K_{kl}(\omega) = \frac{|S_{V_kV_l}(\omega)|}{\sqrt{S_{V_k^2}(\omega)S_{V_l^2}(\omega)}}, \quad (1)$$

where $k, l = x, y, z$. However, for narrowband (harmonic) time realizations of signals, it is convenient to use the standard function of the normalized correlation, which at frequency ω is calculated at time instant t corresponding to the current values ($x(t)$, $y(t)$, z = const, and is averaged in the interval $\tau = nT$, where $T = 1/f$, f is the frequency of the sound signal, $n = 5$–10. Under such conditions, for a four-component (in a certain sense, four-dimensional) vector-scalar sound field, it is necessary to calculate three normalized correlation functions:

$$R_l(\omega, r, t) = \frac{\overline{P(\omega,t)V_l^*(\omega,t)}}{\sqrt{\overline{P(\omega,t)P^*(\omega,t)}\,\overline{V_l(\omega,t)V_l^*(\omega,t)}}}, \quad (2)$$

where the bar above the product means statistical averaging in the interval τ, and $P^*(\omega, t)$ and $V_l^*(\omega, t)$ are the complex conjugate values of the sound pressure and vibration velocity projections. It is obvious that $R_l(\omega, r, t) = \mathrm{Re}R_l(\omega, r, t) + \mathrm{Im}R_l(\omega, r, t)$, where Re and Im

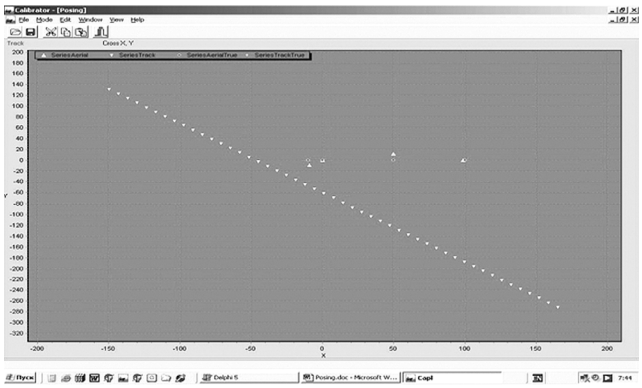

Fig. 1. Results of positioning towed complex with respect to spatially separated receiver vector-scalar modules.

are the real and imaginary parts of the complex correlation function.

Separate experimental results of studying noise correlation using vector receivers are presented in [2, 3]. The results of calculating the spatial and mutual correlation of scalar and vector noise (sea noise) at a point and at the aperture of differently oriented vector-scalar arrays are analyzed in [4]. Experimental studies of the correlation of sound and infrasonic signals at the output of vector-scalar receivers (VSRs), including inertial sensors, were carried out in [2, 3, 5].

One can see that the correlation characteristics of signal and noise fields have been studied insufficiently, and the experimental data discussed in the literature have been obtained, as a rule, in poorly controlled conditions. For example, the authors of [2, 3] study the correlation properties of signals formed in a waveguide from passing ships having complex and unknown amplitude and phase directivity patterns, as well as an undefined motion trajectory with respect to the receiver modules.

Below we study the correlation characteristics and wave spectra of scalar and vector fields using sources towed along a given rectangular trajectory with controlled coordinates. The models of emitted signals are also given in digital form from a computer.

The experiments were conducted in a calibrated waveguide using a universal time system and high-accuracy positioning system. Direction finding of the moving source was carried out simultaneously with a study of the efficiency of suppressing signals from a strongly noise-emitting source using the formed cardioids. We also obtained preliminary results of the distance dependences of the signal arrival (grazing) angles.

EXPERIMENTAL

Let us consider the correlation characteristics of sound fields, the interference structure, and wave spectra of low-frequency tonal signals at frequencies of 117, 320, and 650 Hz. The correlation characteristics were obtained while towing monopole-type electromagnetic emitters located on a combined towed housing, which was also equipped with an underwater container holding power amplifiers, a computer, high-frequency quartz clocks, a control hydrophone, and sensors to record the water temperature and towing depth. In addition to the low-frequency electromagnetic emitters on the combined housing, there was also a medium-frequency pulse emitter (a pinger), which was used to refine the coordinates of the emitters relative to the receiver modules, as well as to estimate the geometry of the location of the receiver modules after their mooring in the water.

The signals from the towed emitters were received in the universal time system simultaneously by the control hydrophone located on the frame of the towed emitting complex and by spatially separated four-component low-frequency (LF) VSRs and high-frequency (HF) VSRs lowered from the research vessel in a bay with a depth of 52–53 m. The remaining three modules (further "water") were raised above the bottom to a height of 20–22 m from the bottom. Note that as vector receivers, we used orthogonally oriented accelerometers built into a spherical housing; they recorded three vibration acceleration vector (VAV) projections ($W_{k,l}$). The VAV projections were calculated by the formula $V_l = -i\gamma W_l(t)$, where $\gamma \sim f^{-1}$ [3].

The universal time system, in addition to two GPS receivers located on board the receiving and emitting ship, also included autonomous quartz clocks submerged in the equipment container. The emitted signals received in real time by the control hydrophone and receiving VSRs were recorded by onboard computers.

Before the start of experimental studies of the correlation characteristics, the receiver modules were put in place. During the experiment, the coordinates of the emitting complex with respect to each of the receiver modules were determined on a real time scale. The coordinates of the receiver modules were refined by acoustic signals from a pinger operating in the frequency range of 2.3–5.2 kHz. Figure 1 shows a computer screen shot of the typical pattern of real-time estimation of the towed emitter coordinates on one of the legs relative to the receiver array [6, 7].

ESTIMATION OF BEARING TO THE MOVING SOURCE

The emitter was towed along rectilinear trajectories, but the traverse distances were set equal to 30 m or more. It was inexpedient for the vessel to pass over the receiver elements, since at a shallow depth, the hydrodynamic field of the ship "rocked" the receiver modules and increased interference. Therefore, to recalculate the real motion trajectories and formation of readings along the direction radial to an element in real time, the range to the towed vehicle was found

using the VAV projections. This made it possible not only to develop a technology for estimating the bearing using VSRs, but also to chose the radial areas of the towing trajectory. For range finding, signals were used that were received by one of the near-bottom VSRs, no. 4. It is assumed that during towing, the spatial orientation of axes V_x, V_y, and V_z of the receiver change insignificantly.

The bearing was estimated by the formula $\theta_n = \arctan \mathrm{Re}\left(\frac{|V_x|}{|V_y|}\right)\exp(i\Delta\varphi)$, where $\Delta\varphi$ is the phase difference between V_x and V_y [3]. Figure 2 shows the results of estimating the bearing from narrowband signals of n realizations at the three frequencies as the towing ship approached or moved away along a radial leg at angles of $\pm\pi/2$.

Note also that in individual areas, sign-changing "overswings" of the bearing estimate are observed, which are explained by the interference structure of the horizontal VAV projections: fluctuations form in the zones of interference minima, for which jumps are typical in the horizontal and vertical projections of the phase gradient and zonal structure of the dependences P, V_x, and V_y and minima ($P_{\max}$). In zones of deep $P_{\min}$ (single points), a phase slue (the phase gradient changes sign) is observed and vorticity is created [8, 9].

Note that with an increase in frequency of a sound signal, the formation rate of particular points (dislocation and saddle) increases, and their coordinates in the horizontal plane are displaced [8, 9].

It is possible to show that when fixing the bearing of wideband signals due to spatial displacement of particular points ($\Delta r/r \sim \Delta\omega/\omega$), fluctuations in the bearing estimate as a result of frequency averaging decrease and overswings are hardly observed at all. In other words, the zones of particular points during wideband processing are "washed out."

ANALYSIS OF THE INTERFERENCE STRUCTURE OF THE CORRELATION CHARACTERISTICS

Figure 3 shows the envelopes of the amplitudes of the sound pressure P and the horizontal V_r component calculated by vector addition in the direction to the moving source of the two horizontal components V_x and V_y using the formula $V_r = V_x\sin(\theta_n) + V_y\cos(\theta_n)$, where θ_n is the bearing to the towed source recorded in real time. To analyze the characteristics of P- and the V_r components, signals from near-bottom VSR no. 4 were also used.

From Fig. 3 it follows that at all frequencies, the shapes of the interference curves for the sound pressure and horizontal component, in addition to the zone near the traverse, practically coincide.

Figure 4, also for the three frequencies, shows the interference curves for sound field P and the vertical vibration velocity component V_z. It is seen that the interference structure of the vertical component is more high-frequency than the dependences in Fig. 3, and the horizontal extent of the zones of the interference maxima is significantly smaller than for the sound pressure or the horizontal VAV projects. The reason is that the vector receiver with the vertical orientation "emphasizes" higher-number modes, and the intervals between the wavenumbers of higher-number modes are larger than for first-number modes; i.e., the wave spectrum broadens. This leads to an increase in irregularity of the interference curves, especially at high frequencies.

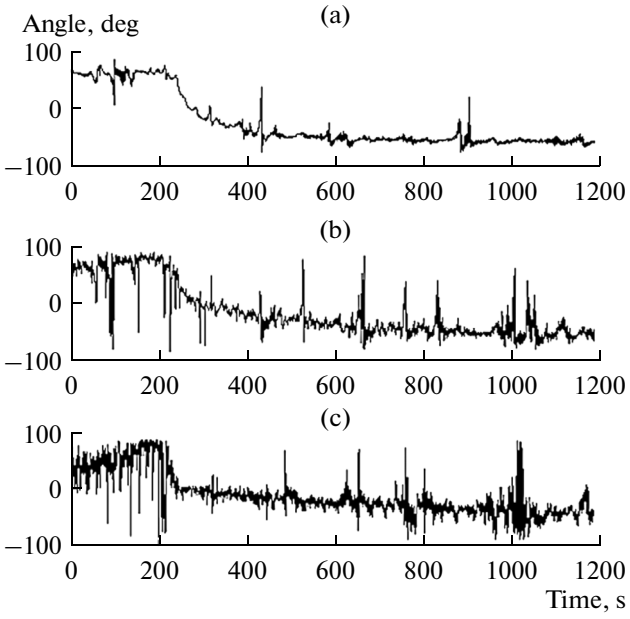

Fig. 2. Bearing to towed source in coordinate system of near-bottom VSR: (a) frequency 117 Hz, (b) frequency 320 Hz, (c) frequency 650 Hz.

The coefficients of correlation between the envelopes of the amplitudes of the sound pressure and horizontal or vertical VAV components (CC_{ro} or CC_{zo}) using (2) for a sequence of n realizations are calculated by the formulas

$$CC_{ro} = \frac{\overline{\left(\sum_n |P||V_r|\right)^2}}{\sum_n |P|^2 \sum_n |V_r|^2}, \quad CC_{zo} = \frac{\overline{\left(\sum_n |P||V_z|\right)^2}}{\sum_n |P|^2 \sum_n |V_z|^2}. \quad (3)$$

The calculated results are given in Tables 1 and 2.

To organize unidirectional reception via the formation of the cardioid directivity characteristic, it is necessary to take into account the phase relations between

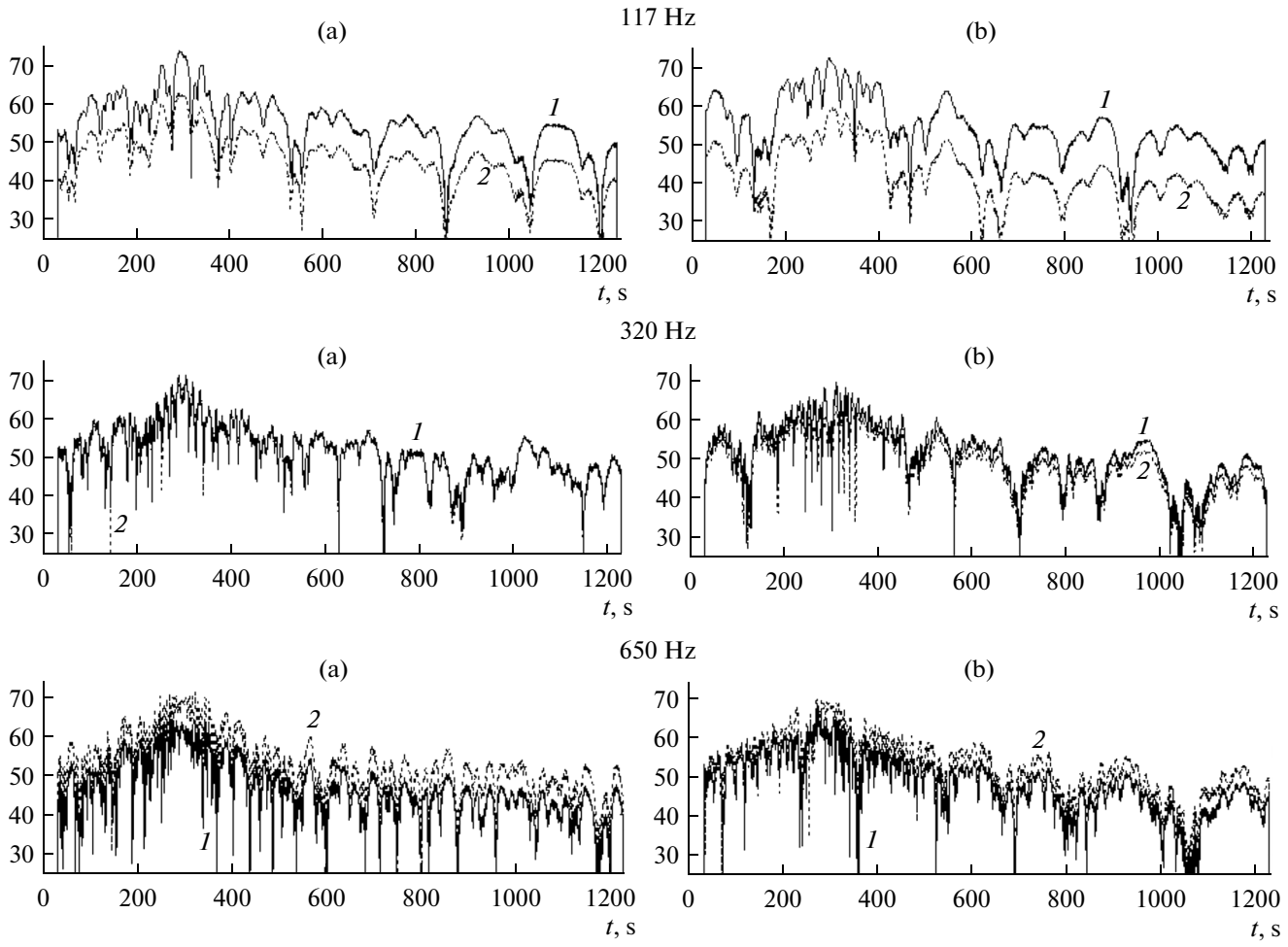

Fig. 3. Interference dependences at frequencies (from top to bottom) of 117, 320, and 650 Hz: *1*, sound pressure P; *2*, V_r component; (a, b) water and near bottom VSR, respectively.

P and V_r. The values of the correlation coefficients of the complex values are calculated by the formula

$$CC_{rk} = \frac{\overline{\left|\sum_n PV_r^*\right|^2}}{\sum_n |P|^2 \sum_n |V_r|^2}. \quad (4)$$

The data for P and V_r are given in Table 3. The calculation results for complex values P and V_z are given in Table 4. Here and below, in Tables 1–4, the correlation coefficients in the initial area of the measurement track correspond to a time interval of 0–192.5 s (C_1); the zone of the traverse, to an interval of 192.5–332.5 s (C_2); and the final part of the measurement track, to an interval of 192.5–1192 s (C_3).

Table 1. Coefficients of correlation between envelopes of amplitudes P and V_r

	C_1	C_2	C_3
117 Hz	0.996	0.986	0.997
320 Hz	0.987	0.920	0.992
650 Hz	0.948	0.870	0.991

From Table 1 it follows that the values of the correlation coefficients with increasing frequency decrease in all time intervals, and the minimum values at all frequencies correspond to regions of the traverse, which is natural, since the sound pressure field at small distances takes into account the entire wave spectrum, including higher-number modes. The vertical component V_r "knocks out" higher-number modes, which at small distances are significant, which leads to a decrease in signal correlation.

With increasing distance, at all frequencies, the values of the correlation coefficients increase. This is explained by the fact that the pressure fields and horizontal VAV components at large distances are formed by the same set of normal waves.

Table 2 shows, for the same time intervals, the values of the coefficients of correlation between the enve-

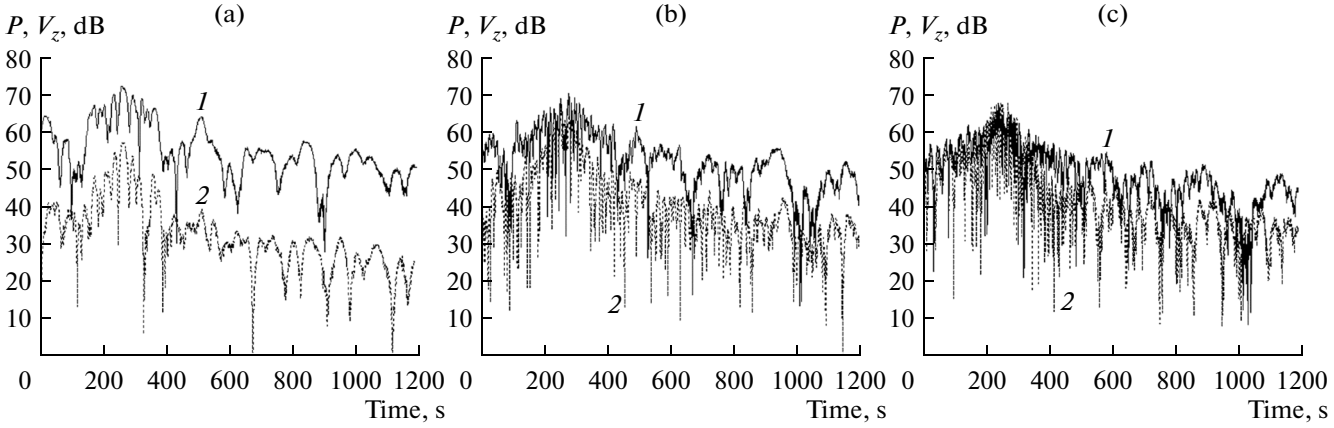

Fig. 4. Interference dependences of sound pressure and vertical VAV component: *1*, pressure *P*; *2*, V_z component; (a) frequency 117 Hz; (b) frequency 320 Hz; (c) frequency 650 Hz.

lopes of the amplitudes of the sound pressure and vertical VAV projection.

Clearly, the characteristics of the correlation coefficients presented in Table 2 differ from the data of Table 1: the maximum values of the correlation coefficients correspond to regions of the traverse, which is explained by the agreement in the near zone of the wave spectra of signals received by the sound pressure receivers and the vertically oriented vector receiver. With distance from the source, the values of the correlation coefficients initially decrease, since differences are formed in the mode composition of signals received by the P and V_z receivers. With a further increase in distance, but under the condition that the measured signal values appreciably exceed the noise value, the similarity of the interference curves improves and quantity CC_{PV_z} increases, since higher-number modes attenuate faster than the energy-carrying first-number modes.

Tables 3 and 4 show the dependences of the correlation coefficients for complex envelopes P, V_r, and V_z. The correlation coefficients CC are calculated for the same time intervals as in Table 1. Clearly, the character of the change in the correlation coefficients of the complex envelopes P and V_r is similar to the dependences of the correlation coefficients of their amplitudes. The dependences of the coefficients of correlation between P and V_z on distance and frequency are similar to the dependences of their amplitudes. However, the values of the correlation coefficients themselves presented in Table 4 are appreciably less than in Table 2. It is also possible to see that with increasing sound frequency, the coefficients of correlation between P and V_r at all distances decrease owing to the influence of different destabilizing factors observed in a real inhomogeneous waveguide, especially in relation to tidal phenomena, as well as in relation to certain deviations in the motion of the towing ship from a rectilinear course. It is significant that the coefficients of correlation between P and V_r for an increase in frequency decrease more slowly, and at individual areas of legs even increase. This is also easily explained by the increase in the contribution of higher-number modes recorded by the vertical VAV component.

ANALYSIS OF THE MODE STRUCTURE OF SCALAR AND VECTOR FIELDS

Figure 5 shows the mode (wave) spectra of signals at the three mentioned frequencies. The spectra were obtained by the standard method—spatial aperture synthesis and FFT over the radial projection of the formed artificial aperture. To take into account the decrease in the influence of the change in the mean signal energy, just like for calculating the CC values, a correction was introduced for the cylindrical deviation of the field. To analyze the wave spectra, we used signals from the water VSR (no. 1) and near-bottom VSR (no. 4).

Clearly the mode spectra of the sound pressure and horizontal vibration velocity component coincide, which confirms the above conclusion on the high correlation of these field components. The mode spectra of the vertical vibration velocity vector differ from the remaining components of the signal field in that the amplitude of the first modes are relatively decreased and the amplitudes of higher-number modes are increased. This conclusion is valid both for the near-bottom and water VSRs.

Table 2. Coefficients of correlation between envelopes of amplitudes P and V_z

	C_1	C_2	C_3
117 Hz	0.738	0.864	0.728
320 Hz	0.655	0.756	0.721
650 Hz	0.749	0.775	0.697

Table 3. Coefficients of correlation between complex envelopes of amplitudes P and V_r

	C_1	C_2	C_3
117 Hz	0.992	0.906	0.953
320 Hz	0.974	0.829	0.829
650 Hz	0.872	0.556	0.793

Table 4. Coefficients of correlation between complex envelopes of amplitudes P and V_r

	C_1	C_2	C_3
117 Hz	0.386	0.634	0.317
320 Hz	0.055	0.450	0.202
650 Hz	0.334	0.354	0.222

As already mentioned above, with an increase in distance from the source, transformation of the wave spectra takes place. With increasing distance, the levels of the low-frequency part of the wave spectra (higher-number modes) decrease (become extinct) quite rapidly and the wave spectra of all four field components—P, V_x, V_y, and V_z—become similar, taking on an identical structure (Fig. 6).

This conclusion is valid for all three frequencies—117, 320, and 650 Hz—at which the experiments were carried out. Sliding spectral analysis, e.g., at a frequency of 117 Hz, made it possible to obtain an estimate for the attenuation coefficients of the higher-number modes. They were 11.6 dB/km for the seventh mode, 6.7 dB/km for the sixth mode, and 2.7 dB/km for the fifth mode. These values are significantly higher than the attenuation coefficients of low-number modes and signals on the whole. Therefore, in the far zone at all frequencies, only the first-number modes remain.

Note that signal processing to isolate the modes was performed in distant areas of the emitter-towing track. For this, areas were chosen with rectilinear motion of the ship or a small change in bearing to the source. In this case, to obtain the radial projections, a correction that takes into account the angle between lines connecting the source and receiver and the direction of the motion trajectory of the source is quite simply introduced with allowance for a change in bearing to the source—by rotating the axes. In addition, to decrease possible shifts and averaging of readings P, V_r, and V_z emitters were towed along radial legs when moving away from or approaching the array, which is confirmed by the virtually constant bearing to the source.

ESTIMATE OF THE EFFICIENCY OF SUPPRESSING STRONGLY NOISE-EMITTING SOURCES

In [3], in analyzing signals from passing ships at a qualitative level, the authors showed that during the formation of a cardioid from the scalar and vector receivers, there is the fundamental possibility of a weakening in the signal value at the output if the cardioid is oriented toward the source according to the zone of the minimum. Such processing is recommended to suppress quite powerful signals from passing ships and other local noise sources, including when detecting weak signals using, e.g., towed vector-scalar arrays [10].

Let us estimate in controlled conditions the efficiency of suppressing strongly noise-emitting sources. The experiment was conducted with constant estimation of the coordinates of the source and receiver, the emitted signals were recorded at different frequencies in the universal time system, the water depth in the emitter-towing area was controlled by echo-ranging, and along the entire towing path it was nearly constant and equal to the depth at the reception point.

To process the algorithm for suppressing noise at the output of the cardioid and increase the suppression efficiency, the cardioid was continuously scanned, which made it possible to take into account small changes in direction to the moving source with time.

Real-time control of the bearing value made it possible for each point at which the emitter was located (in areas corresponding to the travers and distance from the receiver) to estimate the total signal at the output of the two generated cardioids. The cardioids were generated by the known formula $K_{1,2} = P \pm \beta V_r$, where β is the correction coefficient equalizing the dimensions and taking into account the difference in the frequency dependences of the sensitivity [3].

For convenience, taking into account the motion of the towing ship along a radial leg (in addition to the zone near the traverse), the minimum of the cardioid directivity characteristic can be formulated using the expression

$$I_{1,2}(\theta) = P(\theta_{1,2}) + V_x(\theta_{1,2})\sin(\theta_{1,2}) + V_y(\theta_{1,2})\cos(\theta_{1,2}) \to \min, \quad (5)$$

where θ_1 and θ_2 are the directions to the start and end areas of the emitter-towing track.

Figures 7a–7c show the signal responses received by the cardioids (I_1 and I_2) for three frequencies (117, 320, and 650 Hz) . The following notation is used: *1*, quantity I_1 corresponding to addition of signals received by the scalar (P) and vector (V_r) channels; *2*, quantity I_2 corresponding to subtraction of signals received by the scalar (P) and (V_r) channels.

Clearly, in the case of signal reception by the cardioid oriented toward the source according to the zone

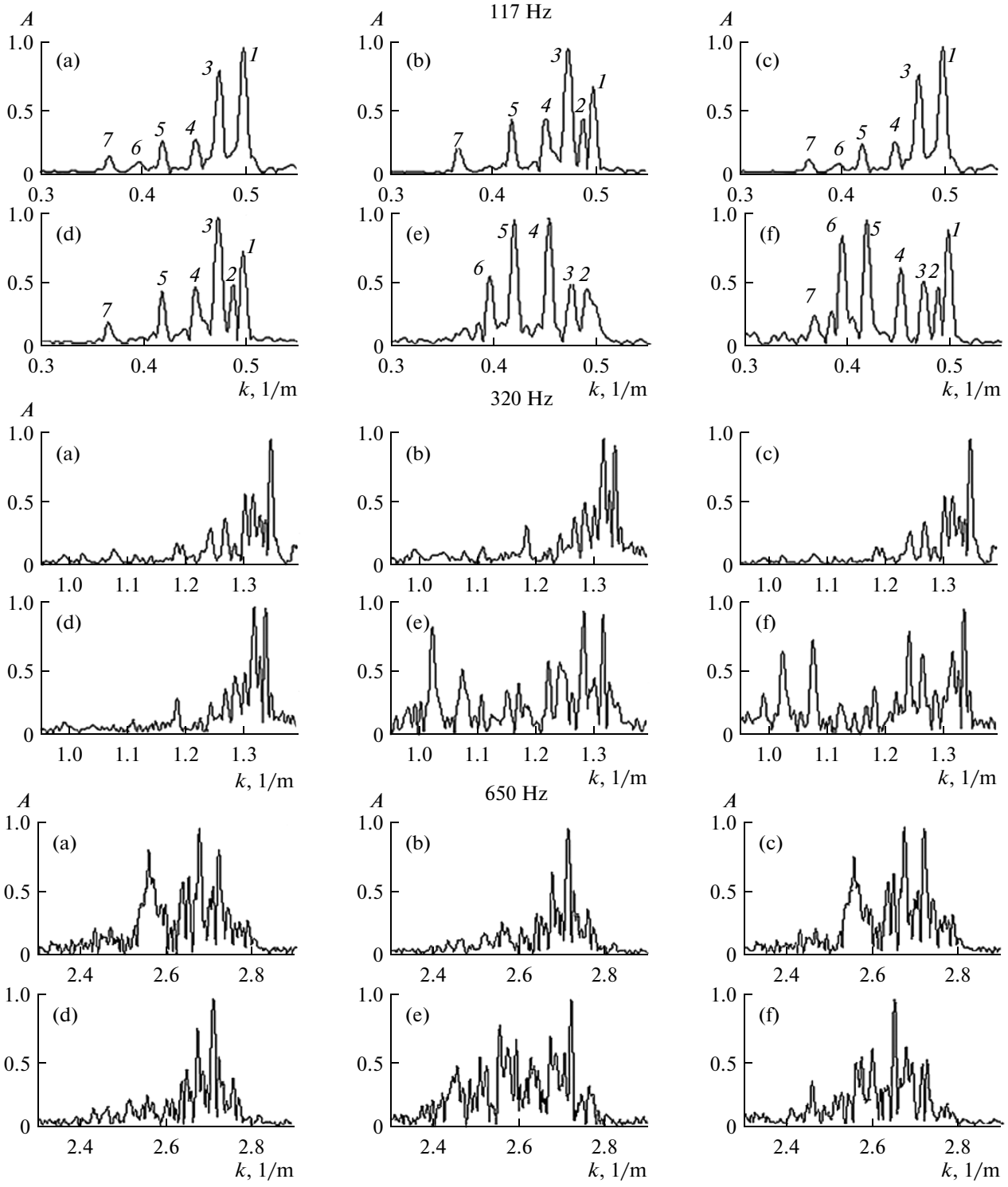

Fig. 5. Normalized wave spectra at frequencies of 117, 320, and 650 Hz: (a, b) sound pressure, (c, d) horizontal VAV component, (e, f) vertical VAV components. Reception depth 33 (a, c, e) and 52 m (b, d, f).

of maximum sensitivity, the response level exceeds by 30 dB or more the value of the signal at the output of the cardioid oriented toward the source according to the zone of minimum sensitivity. Hence it follows that strongly noise-emitting sources during spatial scanning can be efficiently suppressed by the orientation of the zone of the minimum of the cardioid toward them. It is significant that suppression is produced not only

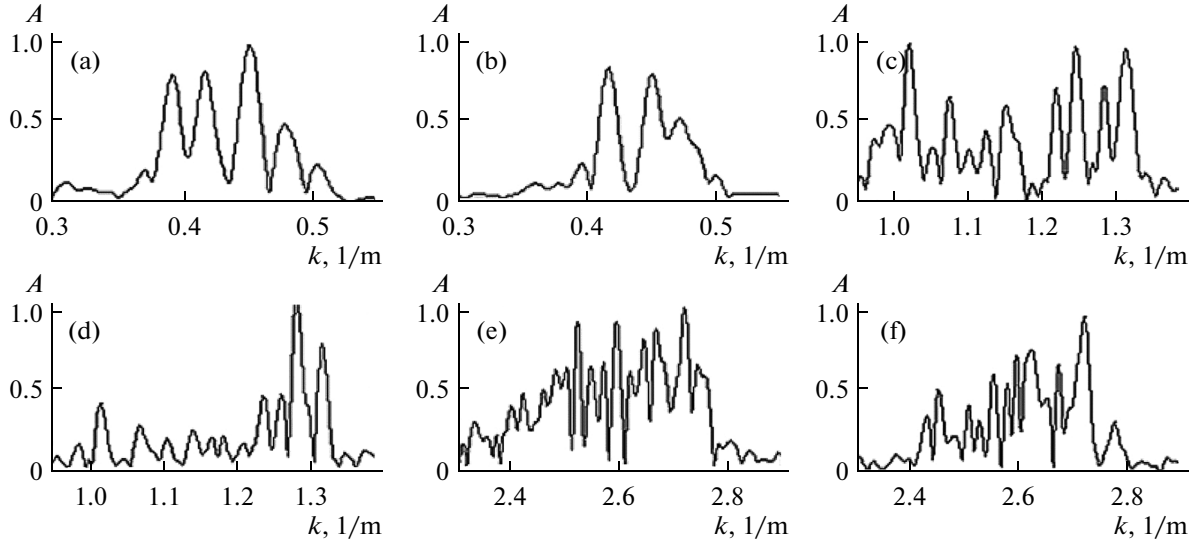

Fig. 6. Normalized wave spectra of vertical VAV component calculated on the first and second half of the measurement track: (a, c, e) first half; (b, d, f) second half; (a, b) 117 Hz, (c, d) 320 Hz, (e, f) 650 Hz.

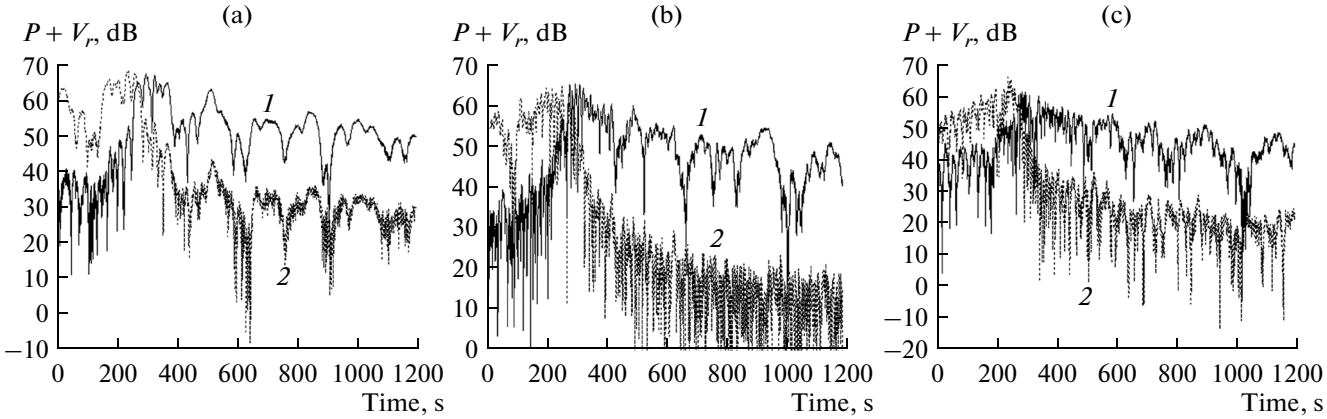

Fig. 7. Signal at vector-scalar module at output of generated cardioid: (a, b, c) frequencies 117, 420, and 650 Hz; *1*, cardioid directed toward departing source according to zone of maximum sensitivity; *2*, cardioid directed at source according to zone of minimum sensitivity.

at individual discrete components, but also simultaneously in a wide frequency band, in which the shape of the cardioid changes insignificantly. It is possible to show that the operating band of the VSR has a value of no less than 10, which significantly exceeds the operating band in which signals are suppressed by the directivity characteristic of the scalar arrays.

VARIATION OF THE VERTICAL ANGLE OF ARRIVAL OF AN EQUIVALENT PLANE WAVE TO THE SIGNAL RECEPTION POINT

The authors of [1, 3] devote attention to the fact that the angle of arrival of a signal in the vertical plane can change in wide limits depending on the sound propagation conditions and the sound signal reception conditions. The authors of [3, 8] recommend using four-component vector-scalar receivers to analyze the angles of arrival (grazing angles) of signals $\varphi(t(r))$ in the vertical plane. For this, simple relations are used in the form $\varphi = \arctan \dfrac{V_z}{\sqrt{V_x^2 + V_y^2}}$. Figure 8 shows for one of the emitter-towing trajectories the dependence of the angle of arrival $\varphi(t(r))$ on time (on distance). Clearly, in individual areas, the angles of arrival taking into account the phase difference V_z with respect to sound pressure P change jumpwise within wide limits, and "discontinuities" are observed. As analysis has shown, these zones correspond to zones of interference minima, which are in complete agreement with the conclusions of [8, 9]. In the zones of interference maxima, the phase gradients are smooth and the angles of arrival are close to the horizontal direction. One can also see that with an increase in frequency, the irregularity of the dependence $t(r)$ also increases, because in the given distance interval, there is an increase in the number of modes and zones of interfer-

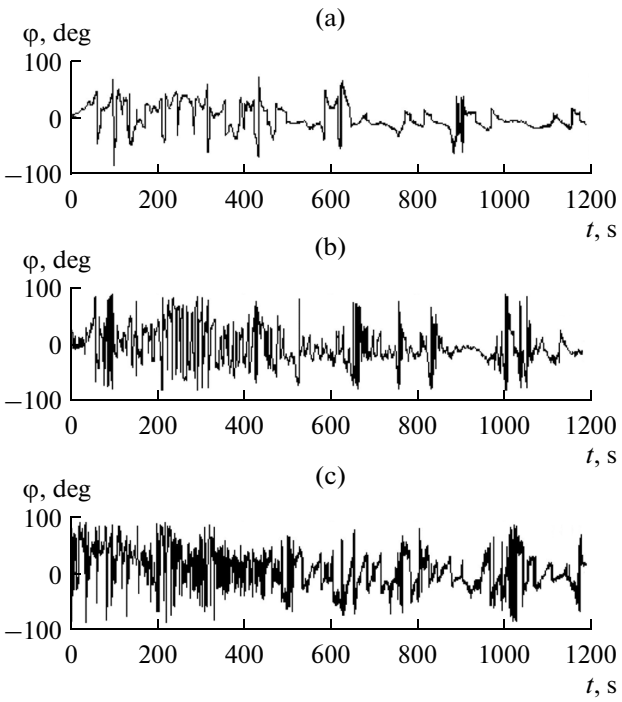

Fig. 8. Angle of arrival of signal in vertical plane: (a) frequency 117 Hz, (b) frequency 320 Hz, and (c) frequency 650 Hz.

ence maxima and minima. This phenomenon requires special additional study.

CONCLUSIONS

Generalizing the results obtained, we can draw the following conclusions.

The correlation coefficients of the sound pressure and horizontal projection of the vibration velocity vector are 0.92–0.99, and the correlation coefficients of the sound pressure and vertical projection decrease to 0.66–0.85. With an increase in distance between the noise source and the receiver, the correlation increases (under the condition that the signal/noise ratio is larger than unity). With an increase in frequency, the correlation for the horizontal projections V_r decreases, and for the vertical projections V_z, it stabilizes.

The mode spectra characteristics substantiate the obtained large values of the correlation coefficients: the mode spectra of the sound pressure and horizontal projection coincide; in the mode spectra of the vertical component, there are also higher-number modes, which with an increase in distance weaken quite rapidly. As a consequence, the coefficients of correlation between the sound pressure and vertical vibration velocity component increase.

When using scalar fields or horizontal vibration velocity projections, three to five normal waves are isolated. When the vertical vibration velocity component is used, seven to nine modes are isolated. Therefore, when acoustically calibrating a waveguide, it is expedient to use not only scalar receivers, but also the vertical VAV component. An increase in the number of isolated modes increases the accuracy and reliability of identifying the parameters of the bottom model.

When it is oriented toward a strongly noise-emitting source according to the zone of the minimum, a cardioid receiver suppresses the received signal by 20–30 dB or more. With range finding and accompaniment of a moving source, it is possible to suppress its signal along the entire motion trajectory.

Estimates for the bearing or angle of arrival (grazing angle) when a source is towed at distances, zones of interference minima differ by the large instability, and sign-changing phase jumps in P, V_r, and V_z are observed in the horizontal and vertical plane.

The presented experimental dependences agree well with the results of computer simulation of the scalar and vector components of the sound field using the calibration results of the test area.

The correlation of signals received by the scalar and vector channels of a VSR is great, which makes it possible to recommend using this effect to substantiate the necessity of creating vector-scalar arrays and detect weak signals. The correlation of the sound pressure and vector components of the main (at least for stationary systems) interference component—sea noise—is small, and in individual cases, it tends to zero. This should lead to an increase in the noise immunity of detection [10].

ACKNOWLEDGMENTS

The authors are pleased to thank the employees of OOO ACK Pro, who participated in preparing technical instruments, carrying out research, and developing software.

REFERENCES

1. R. J. Urick, *Principles of Underwater Sound* (McGraw-Hill, 1975; Sudostroenie, Leningrad, 1978).
2. V. A. Shchurov, *Vector Acoustics of the Ocean* (Dal'nauka, Vladivostok, 2003) [in Russian].
3. V. A. Gordienko, *Vector–Phase Methods in Acoustics* (Fizmatlit, Moscow, 2007) [in Russian].
4. G. M. Glebova, G. N. Kuznetsov, and O. E. Shimko, Acoust. Phys. **59**, 453 (2013).
5. V. I. Korenbaum, Acoust. Phys. **41**, 825 (1995).
6. A. I. Belov, A. P. Buyanov, G. M. Glebova, G. N. Kuznetsov, O. K. Morev, and A. V. Semenov, in *Proc. 28th Sess. Russ. Acoust. Soc., 2004*, vol. 2, pp. 196–199.
7. G. N. Kuznetsov and G. M. Glebova, Phys. Vibr. **9**, 235 (2001).
8. V. A. Eliseevnin and Yu. I. Tuzhilkin, Acoust. Phys. **47**, 688 (2001).
9. V. M. Kuz'kin, A. V. Ogurtsov, and V. G. Petnikov, Acoust. Phys. **44**, 77 (1998).
10. A. V. Aver'yanov, G. M. Glebova, and G. N. Kuznetsov, Acoust. Phys. **57**, 696 (2011).

Translated by A. Carpenter